Viscoplastic and Granular Behavior in Films of Colloidal Nanocrystals

Dongyun Lee,[1,2] Shengguo Jia,[2,3] Sarbajit Banerjee,[2,3] Joze Bevk,[2,3] Irving P. Herman,[2,3] and Jeffrey W. Kysar[1,2,*]

[1]*Department of Mechanical Engineering, Columbia University, New York, New York 10027, USA*
[2]*Materials Research Science and Engineering Center, Columbia University, New York, New York 10027, USA*
[3]*Department of Applied Physics and Applied Mathematics, Columbia University, New York, New York 10027, USA*

(Received 3 October 2006; published 9 January 2007)

Nanoindentation measurements of electrophoretically deposited films of colloidal CdSe nanocrystals, capped by organic ligands, show the films have an elastic stiffness modulus of ~10 GPa and exhibit viscoplasticity. This mechanical response suggests polymeric features that are attributable to the ligands. After particle cross-linking and partial ligand removal, the films exhibit more features of granularity.

DOI: 10.1103/PhysRevLett.98.026103 PACS numbers: 81.07.−b, 61.46.Hk, 68.60.Bs, 81.20.−n

Colloidal nanocrystals are composed of inorganic nanoparticle cores with organic ligands bound to the surface of each core. We have previously demonstrated that electrophoretic deposition is a convenient way to deposit high quality, uniform films of nanoparticles from a solvent solution either over large areas or, selectively, in patterned regions [1]. These films can be considered a new class of ''interfacial solids'' with the interfaces consisting of bonds between inorganic cores and organic ligands. The complex interplay between the nature and strength of these bonds, the ligand-ligand dynamics, and residual solvent trapped in the nanopores, is expected to greatly affect the film properties, in particular, the mechanical behavior. A well-known characteristic of these and of dry cast nanocrystal films is that the drying process induces high residual stresses that lead to a rich variety of cracking patterns in films above a certain critical thickness. The dependence of both elastic and plastic mechanical properties on deposition conditions and interfacial chemistry needs to be understood to control and optimize the film mechanical behavior and stability.

In this Letter, we show that nanoindentation measurements provide valuable information about the film's mechanical behavior for the model systems of CdSe nanocrystal films; the results can be validated by other experimental methods. Corresponding numerical simulations further elucidate the role the ligands play in the overall mechanical behavior of the films and point to the deformation modes during plastic flow.

Monodisperse CdSe nanocrystals capped by trioctylphosphine oxide (TOPO) and trioctylphosphine (TOP) ligands were prepared as in Ref. [2], with core diameter 3.2 nm. After the particles were reprecipitated twice [3], smooth films of these nanocrystals were formed on Au films (150 nm) atop Cr (10 nm) on c-Si by electrophoretic deposition (EPD) [1] from a solution of these particles in a hexane/octane solution (volume ratio 90%/10%), to form 600–3200 nm-thick films with ~1 cm lateral dimensions (Table I). Films thicker than ~800 nm exhibited channel cracks [1]; films thinner than ~800 nm showed no cracks, but had elastic strain due to solvent evaporation after EPD. The 600 nm-thick films were also examined after baking (30 min at 70 °C in N_2), cross-linking (1 mM 1,7-heptanediamine in methanol for 4 h followed by baking 30 min at 70 °C in N_2), and soaking in acetone (5 min) [3].

Nanoindentation experiments were conducted with an MTS Nanoindenter® II under displacement control to no more than ~30% of the nanocrystal film thickness. Figure 1 shows average force-displacement data for a 1000 nm-thick film. At a given force level, data are averaged from at least 15 indentations, with scatter indicated by standard deviation in displacement. The displacement rate during the indentation was either 5 nm/s or 10 nm/s to a predetermined load, followed by a constant load dwell for either 10 or 20 s. Unloading was under displacement control at the same rate as the indentation.

The elastic stiffness modulus E was determined from the unloading slope. The continuous stiffness measurement technique [4] allows the unloading slope to be determined as a function of depth by superimposing a dither on the displacement. As will be discussed further below, the presence of the underlying substrate, which has a higher elastic stiffness than the film, leads to unloading slopes greater than those expected in a bulk specimen of the same material. This is known as the substrate effect which, if not accounted for properly, leads to spurious values of E; such

TABLE I. Elastic stiffness modulus E and hardness H were obtained at a deformation of 10% of the film thickness for each film at the two deformation rates shown. The stated uncertainty denotes the standard deviation of the results taken at different points probed. The 500 nm, soaked film is the 600 nm film after baking, linking, and soaking.

Film	5 nm/s		10 nm/s	
	E, GPa	H, MPa	E, GPa	H, MPa
3200 nm	8.0 ± 0.4	350 ± 50	8.4 ± 0.3	400 ± 30
1000 nm	9.8 ± 1.6	440 ± 80	11.9 ± 1.4	600 ± 80
600 nm	9.9 ± 1.3	380 ± 90	9.8 ± 1.6	380 ± 90
500 nm, soaked	2.0 ± 0.5	120 ± 40	2.5 ± 0.7	210 ± 90

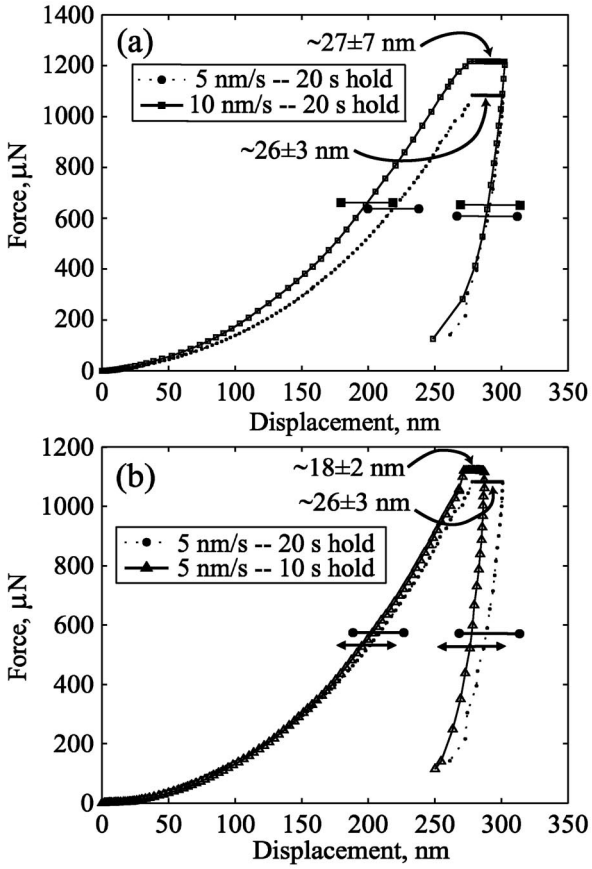

FIG. 1. Force vs displacement curves of 1000 nm-thick CdSe nanocrystal EPD films with (a) 5 nm/s or 10 nm/s displacement rate and 20 s hold time at peak load, and (b) 5 nm/s displacement rate and 10 s or 20 s hold times at peak load. Average displacement is plotted for a given force for each load cycle of a curve (increasing displacement, constant load, decreasing displacement), with the value of the displacement at constant load given on the plot. Error bars indicate the standard deviation in displacement at a given force.

erroneously high values of E will be referred to here as the *apparent* elastic stiffness. The hardness H of the film was determined as the ratio of the indentation force to the projected area of contact on the original surface [4]; the hardness is independent of indentation depth for these experiments. Initial nanoindentation studies indicated no systematic variations of E and H with respect to position of the indent relative to the channel cracks, showing that the mechanical properties do not appear to be sensitive to variations in elastic residual strain and the small amount of delamination near channel cracks; the more extensive studies presented here were made far away from cracks. Table I lists the values of E and H for various films of different thickness and post-deposition treatments, obtained at an indentation depth of 10% of the film thickness to minimize substrate effects. A typical atomic force microscope (AFM) image of an indentation is shown in Fig. 2. No additional cracks were induced as a consequence of indentation in films of thicknesses 1000 nm and less.

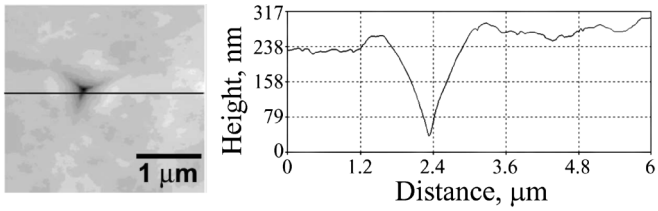

FIG. 2. AFM image and scan of an indent in a 600 nm-thick film.

The slopes of the loading curves in Fig. 1 increase with the strain rate, which indicates a strain rate dependence of constitutive relations, and therefore viscoplastic behavior (as is commonly seen in polymers) and/or viscoelastic behavior (for which the strain is reversible). The significant permanent deformation in the material following removal of the indenter suggests it is predominantly viscoplastic. Time dependence is also evident in the larger displacements during the constant load phase with longer dwell times in Fig. 1. In polymers, the rate dependence of plastic deformation and creep (i.e., viscoplastic properties) originates from the thermally assisted deformation mechanism of detachment, sliding, and reattachment of polymer chains, which in the present case corresponds to ligand-ligand interactions.

A continuum model of deformation by a nanoindenter tip is used to analyze the film mechanical properties; this is appropriate because the depth and width of the indented region (with radius of curvature ~150 nm) are very much larger than the interparticle spacing (~ 5 nm). The films contain a random distribution of CdSe cores with polymer-like TOPO and TOP capping ligands. If no ligands were present, the films would consist entirely of randomly packed nanoparticles and the mechanical properties would likely exhibit some characteristics of a granular material. However, since the nanoparticles are capped by polymer-like capping ligands, it is expected that the films exhibit properties of both polymers and granular materials. The relative degree of polymeric or granular behavior is unknown *a priori*, and therefore a film constitutive model is employed which is able to capture characteristics of both classes of materials.

The mechanical properties of polymers and granular materials have important similarities and differences. During irreversible deformation, plastic strain in polymers is nearly isochoric (i.e., incompressible, which implies that the trace of the plastic strain tensor can be approximated as zero). In contrast, plastic deformation in densely packed granular media is often accompanied by dilation (or permanent volumetric strain), because neighboring grains must slide around and past each other (which requires a larger volume). The relationship between an increment of permanent volumetric strain $\delta\varepsilon_\nu$ and the corresponding increment in plastic shear strain $\delta\gamma$ can be expressed as $\tan\psi = \delta\varepsilon_\nu/\delta\gamma$, where ψ is the so-called dilation angle. Values of ψ in granular media range from 0° for clays to

15° for dry densely packed sand [5]. Loosely packed granular materials can be compacted (i.e., negative dilation) upon plastic deformation.

The yield stress of both polymers and granular materials undergoing irreversible deformation is a function of pressure. The relationship is often assumed to be linear (Drucker-Prager model [6]); thus the criterion for applied stress (here expressed as the von Mises equivalent stress, t) at the initiation of plastic deformation is $t = \sigma_y^0 + P\tan\beta$, where P is the scalar pressure. ($P = -J_1/3$, where J_1 is the first invariant of the Cauchy stress tensor σ, and $t^2 = J'_2$ is the second invariant of the deviatoric stress tensor defined as $s = \sigma + PI$, with I the unit second rank tensor.) In the granular media literature, β is called the friction angle and in the polymer literature, $\tan\beta$ is called the pressure sensitivity. Typical friction angles for both polymers and granular media are in the range of 5° to 20°. The yield stress is related to the hardness by H/N, where N is typically 3 for metals, 1 for porous materials, 1.5 for oxide glasses, and 2 for polymers [7]. The yield stress at zero pressure, σ_y^0, is modeled using H from Table I, with N set at 2 because the ligands are polymeric.

The strain hardening behavior of different classes of materials varies widely, but general trends exist. Polymers typically exhibit strain softening upon attainment of yield, which is accompanied by shear banding (or localization of deformation); however, the localizations are often suppressed because of rehardening from alignment and reattachment of the polymer chains [8]. Granular materials also exhibit shear localization because of strain softening associated with locally dilated regions. Stabilization of the localization does not occur as readily in granular media, especially if there is dry contact between adjoining grains.

Polymers have rate-dependent constitutive properties, even at sufficiently small strain rates for which inertial effects can be neglected, whereas those of dry granular materials are not typically as highly rate dependent. The time-dependent aspects of the plastic deformation are modeled using the phenomenological power-law relationship that relates the strain rate $\dot{\gamma}$ to the applied stress as $\dot{\gamma} = At^n$, where A and n are constants [9]. The elastic properties are assumed to be independent of pressure and deformation.

The simulation was performed using the general purpose commercial finite element program ABAQUS [10]; the constitutive properties and deformation quantities were suitably generalized to account for finite deformations. The three-sided Berkovich indenter was modeled as a rigid axisymmetric cone [11] with included angle of 140.6°, and truncated with a 150 nm tip radius of curvature [12]. Coulomb friction between the indenter tip and the film was assumed, with a coefficient of 0.2; the simulations were not very sensitive to this value. The axisymmetric element employed was a CAX4RH with enhanced hourglass control. The simulations were performed at constant indentation rate to a prescribed force, followed by a dwell at that force, followed by a withdrawal of the indenter at the same displacement rate as the initial indentation. The simulated film was 1000 nm-thick, and the underlying Au and Cr films as well as the silicon substrate were accounted for in the simulations. The parameters E (9.8 GPa) and H (440 MPa) were obtained from Table I for a displacement rate of 5 nm/s; the value of Poisson's ratio ν (0.3) was assumed. Since no gross evidence of shear localizations was present (c.f. Fig. 2) near the indentations for the loads considered, it was assumed that negligible strain softening occurred so the value of σ_y^0 ($= H/2$) was held constant throughout the simulation. The friction angle β, dilation angle ψ, and the creep law parameters n and A were determined by fitting the results of the simulation to experiment. The fit is sensitive to the first three parameters, but not to the fourth.

Figure 3(a) shows the results of the simulations for the 1000 nm-thick film in which the displacement rate is 5 nm/s and the dwell time is 20 s, with $\beta = 15°$, $\psi = 5°$, $n = 2.85$, and $A = 1 \times 10^{-9}$ s^{-1}(MPa)$^{-n}$; the simulated force-displacement trace lies well within the experimental uncertainty. The shape of the initial part of the curve is sensitive to both the friction angle and the creep exponent, whereas the dwell portion of the curve is very sensitive only to the creep exponent. The unloading portion of the curve depends upon the elastic response. Although the mechanical parameters obtained do not constitute a unique set, good fits were obtained only with at most small variations about these values.

In addition, it is possible to compare the apparent E vs depth curve and the H vs depth curve against experiment as in Figs. 3(b) and 3(c), respectively. The increase of apparent stiffness with indentation depth in Fig. 3(b) was caused mainly (but not all) by the presence of the underlying silicon substrate which has a greater stiffness than the film. This was verified by simulations of indentation in a bulk material of the same properties also shown in Fig. 3(b), which show only slight variation of apparent stiffness as a function of depth. It should be noted that the small offset between the calculated and the experimentally measured apparent stiffness in Fig. 3(b) is caused by differences in the shape of the indenters used in the simulations and experiments. These model parameters also simulate well the response at the various indentation rates and dwell times for other cases of the 1000 nm film and also for the 600 nm film.

The very low value of the dilation angle (5°) suggests that the nanocrystal films have more of a polymeric character than a granular character. This is supported by the observation that there is no evidence of localized shear bands associated with the indentations, as in Fig. 2.

The elastic modulus is much smaller for the cross-linked films after soaking (2.0–2.5 GPa, vs ~10 GPa, Table I) and it does not apparently increase with depth of indentation. This suggests that soaking removes many of the

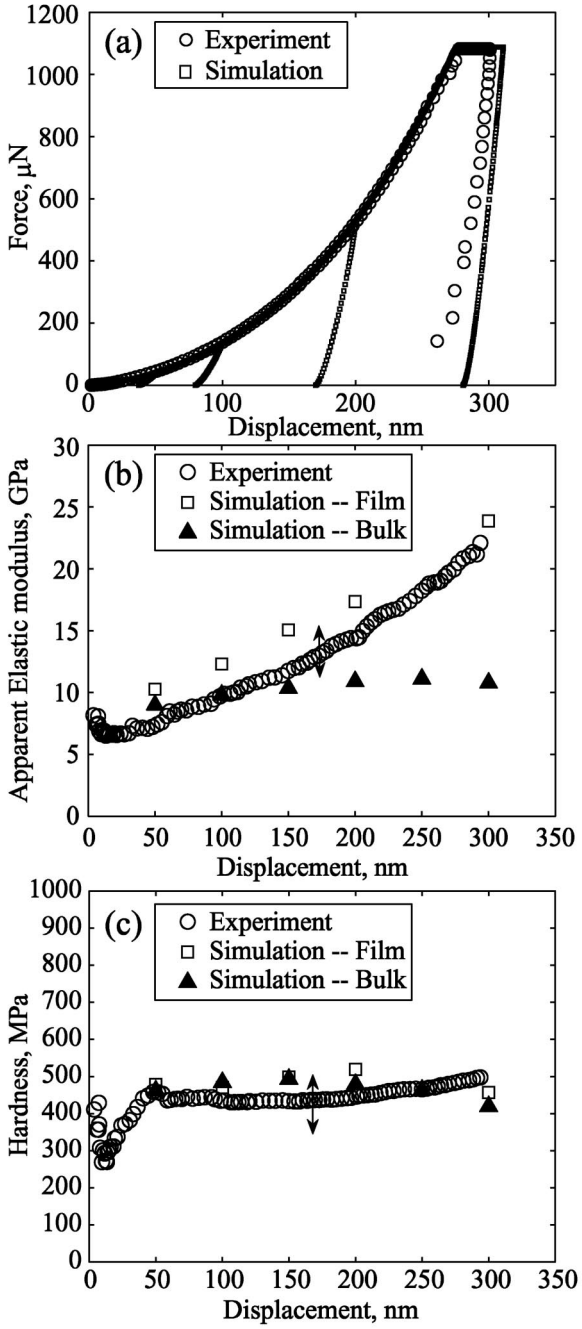

FIG. 3. Simulation results for a 1000 nm-thick CdSe nanocrystal film on the Au/Cr/Si substrate loaded at 5 nm/s with a hold time of 20 s, are compared to experiment for (a) force-displacement curves, (b) average apparent E vs displacement, and (c) average H vs displacement. In (b) and (c), vertical bars represent standard deviation of average apparent E and H, and simulations are also shown for a semi-infinite medium of CdSe nanocrystals (no substrate, "bulk"); the difference between apparent E from experiment and simulation can be attributed to uncertainties in modeling the nanoindenter tip.

ligands, leaving mostly the relatively low density of cross-linking connections between nanocrystals. The CdSe nanoparticles are subject to compaction when a load is applied, which would explain why the apparent elastic stiffness does not increase with indentation depth. Therefore such a film exhibits the compaction behavior of a loosely packed granular material. The hardness of this film is also much smaller.

The value of the elastic modulus previously deduced indirectly via Raman spectroscopy of the CdSe cores under tension for the 3200 nm EPD film described in Table I (9.7 GPa, assuming $\nu = 0.3$) [13] is very similar to that measured here via nanoindentation (~ 8 GPa) in which the deformation is largely compressive.

In conclusion, nanoindentation shows that the mechanical response of electrophoretically deposited films of colloidal CdSe nanocrystals exhibit viscoplasticity, suggesting polymeric features that are attributable to the organic ligands bound to the nanocrystal cores; with fewer ligands, features of deformation consistent with granular media emerge. The findings concerning the relative degree of polymeric and granular behavior should apply to films of other core or ligand nanocrystals, other methods of nanocrystal film formation, and to ordered nanocrystal arrays.

This work was supported primarily by the MRSEC Program of the National Science Foundation under Grant No. DMR-0213574 and the New York State Office of Science, Technology and Academic Research (NYSTAR), and partially by NSF under No. CMS-0134226 and NSEC No. CHE-0641523. Nanoindentation studies at the ORNL SHaRE User Center were sponsored under No. DE-AC05-00OR22725. The authors thank G. M. Pharr and S. H. Shim for their valuable advice and L. Brus for use of his synthesis facilities.

*Electronic address: jk2079@columbia.edu

[1] M. A. Islam and I. P. Herman, Appl. Phys. Lett. **80**, 3823 (2002).
[2] C. B. Murray, D. J. Norris, and M. G. Bawendi, J. Am. Chem. Soc. **115**, 8706 (1993).
[3] M. A. Islam, Y. Xia, D. A. Telesca, Jr., M. L. Steigerwald, and I. P. Herman, Chem. Mater. **16**, 49 (2004).
[4] W. C. Oliver and G. M. Pharr, J. Mater. Res. **19**, 3 (2004).
[5] P. A. Vermeer and R. de Borst, Heron **29**, 1 (1984).
[6] D. C. Drucker and W. Prager, Q. Appl. Math. **10**, 157 (1952).
[7] D. M. Marsh, Proc. R. Soc. A **279**, 420 (1964).
[8] M. C. Boyce, D. M. Parks, and A. S. Argon, Mech. Mater. **7**, 15 (1988).
[9] F. H. Norton, *The Creep of Steel at High Temperatures* (McGraw-Hill, New York, 1929).
[10] *ABAQUS 6.4 User's Manual* (ABAQUS Inc., Pawtucket, RI, 2004).
[11] G. M. Pharr and A. Bolshakov, J. Mater. Res. **17**, 2660 (2002).
[12] H. Bei, E. P. George, J. L. Hay, and G. M. Pharr, Phys. Rev. Lett. **95**, 045501 (2005).
[13] S. Banerjee, S. Jia, D. I. Kim, R. D. Robinson, J. W. Kysar, J. Bevk, and I. P. Herman, Nano Lett. **6**, 175 (2006).